Astron. Astrophys. 320, 19–25 (1997)

ASTRONOMY
AND
ASTROPHYSICS

Variability in the synchrotron self-Compton model of blazar emission

A. Mastichiadis and J.G. Kirk

Max-Planck-Institut für Kernphysik, Postfach 10 39 80, D-69029 Heidelberg, Germany

Received 17 July 1996 / Accepted 25 September 1996

Abstract. We present a model of the spectra of gamma-ray emitting blazars in which a single homogeneous emission region both emits synchrotron photons directly and scatters them to high (gamma-ray) energy before emission (a 'synchrotron self-Compton' or SSC model). In contrast to previous work, we follow the full time dependent evolution of the electron and photon spectra, assuming a power-law form of the electron injection and examine the predictions of the model with regard to variability of the source. We apply these computations to the object Mkn 421, which displayed rapid variability in its X-ray and TeV emission during a multiwavelength campaign in 1994. This observation strongly implies that the same population of electrons produces the radiation in both energy bands. By fitting first the observed quiescent spectrum over all 18 orders of magnitude in frequency, we show that the time dependence of the keV/TeV flare could have been the result of a sudden increase in the maximum energy of the injected electrons. We show also that different types of flare may occur in this object and others, and that the energy band most sensitive to the properties of the acceleration mechanism is the X-ray band.

Key words: galaxies: active – BL Lac objects: Mkn 421 – galaxies: jets – X-rays: galaxies – Gamma rays: theory

1. Introduction

Mkn 421 is a nearby (z=0.03) BL Lac object, with emission characterised by variability at all wavelengths. It appears to emit purely non-thermal continuum radiation; emission lines are absent. In addition, Mkn 421 is the first extragalactic source which has confirmed detections in TeV $\gamma-$rays (Punch et al. 1992, Schubnell et al. 1996). It is also one of the $\sim$50 active galactic nuclei (AGN) to have been detected by the EGRET experiment on the Compton Gamma-Ray Observatory (von Montigny et al. 1995).

Concerted efforts have been undertaken to obtain simultaneous observations of blazars over a wide spectral range. In April and May 1994, Mkn 421 was the target of such an observation (Macomb et al. 1995, 1996). This object had been observed in previous multi-wavelength campaigns (Brodie, Bowyer & Tennant 1987, Makino et al. 1987) but the 1994 campaign was the first to cover both the GeV and TeV gamma-rays as well as the radio to X-ray bands. Furthermore these coordinated observations were fortunate to coincide with an increase in the flux above 250 GeV by a factor of several in a few days. Contemporaneous observations performed by ASCA showed the X-ray flux was also in a high state compared to earlier observations. Significantly, EGRET did not detect a flare in the MeV-GeV regime, nor was any change observed in the radio to optical bands. These results imply that a single population of electrons is responsible for the radiation in both the keV and TeV bands and provide a potential test for the theoretical models that have been put forward to explain the emission from AGN (e.g., Maraschi, Ghisellini & Celotti 1992, Dermer & Schlickeiser 1993, Sikora, Begelman & Rees 1994, Blandford & Levinson 1995, Marcowith, Henri & Pelletier 1995).

One of the most promising models for the emission mechanism of BL Lac objects (including Mkn 421) is the "synchrotron self-Compton model" (SSC). Originally applied to nonthermal emission of frequency up to X-rays (Jones, O'Dell & Stein 1974), this mechanism has been revised to accommodate the recent discoveries by EGRET and WHIPPLE. The generic picture is that the radio to X-ray photons arise as the synchrotron radiation of relativistic electrons accelerated by some unspecified mechanism in a blob of plasma which itself moves relativistically outwards from the core of the AGN; the gamma-rays are the result of the inverse Compton scattering of the synchrotron photons by the relativistic electrons in the blob. Several expositions of the steady state spectrum predicted by this model can be found in the literature. Variability is also predicted in these models, where it arises not from a non-steady electron distribution but from changes in the parameters of the source as it moves through the jet (Celotti, Maraschi & Treves 1992, Maraschi, Ghisellini & Celotti 1992, Bloom & Marscher 1996).

However, during a flare, the electrons may not have time to reach a steady state since their cooling time can be much longer than the timescale of the flare. This in turn means that

Send offprint requests to: J.G. Kirk

in order to follow the evolution of a multifrequency flare such as detected during the 1994 campaign, time dependent calculations, taking into account electron injection and cooling and following the evolution of the spectrum, are indispensable. In this paper we present such a calculation. Sect. 2 contains a brief description of the computational method; in Sect. 3 we compare the predictions of our model to the multiwavelength spectrum of Mkn 421 and show the time dependent evolution of flares obtained by varying certain parameters in the injected electron spectrum. We conclude in Sect. 4 with a discussion of our results.

2. Computational model

As part of a general approach to the modelling of AGN spectra, including the self-consistent acceleration of a hadronic component, we have developed a numerical code capable of following the time evolution not only of the proton, but also of the photon and electron distributions in the source (Mastichiadis & Kirk 1995, henceforth MK95). To accomplish this, we assumed each component can be represented by a spatially averaged distribution, treating escape from the source by a simple 'catastrophic loss' term. The system of three time-dependent kinetic equations for the distributions as functions of energy is then amenable to numerical solution. The relevant physical processes taken into account for the electron and photon distributions include synchrotron radiation, inverse Compton scattering both in the Thomson and Klein Nishina regimes, as well as photon-photon pair production and synchrotron self-absorption. Other processes included in the original code, such as pair annihilation and photon downscattering on cold electrons, turn out to be irrelevant for the case we are considering here.

Two minor modifications must be made before this code can describe the SSC model for blazars. Firstly, since the acceleration mechanism is not directly addressed, it is not necessary to follow the proton distribution. Instead, an arbitrary dependence of the electron injection function on energy and time can be implemented. Secondly, the extremely high flux of gamma-rays observed from blazars indicates that the source must be Doppler-boosted. Thus, quantities such as the photon spectrum, which are computed in the rest frame of the source, require a Lorentz transformation into the observer's frame.

With these changes, the parameters which specify the source are as follows:

- the Doppler factor $\delta = 1/[\Gamma(1-\beta\cos\theta)]$, where Γ and $c\beta$ are the Lorentz factor and speed of the blob, and θ is the angle between its direction of motion and the line of sight to the observer,
- the radius R of the source (in its rest frame, in which it is assumed spherical) from which the crossing time $t_{\rm cr} = R/c$ can be defined; the variation timescale in the galaxy frame is then given by $t_{\rm var} = R/(\delta c)$,
- the magnetic field strength B, specified in units of the critical magnetic field: $b = B/(4.414\times10^{13}\,{\rm G})$. When combined with R, this determines the magnetic "compactness" which can be defined in analogy with the photon compactnesss (MK95) as $\ell_{\rm B} = \sigma_{\rm T}RB^2/(8\pi m_{\rm e}c^2)$, where $\sigma_{\rm T}$ is the Thomson cross section and $m_{\rm e}$ the electron rest mass,
- the electron injection spectrum, for which we take $Q_{\rm e} = q_{\rm e}\gamma^{-s}e^{-\gamma/\gamma_{\rm max}}$ where γ is the electron Lorentz factor. The three scalar parameters used to specify this distribution in the following are s, $\gamma_{\rm max}$ and the electron injection compactness $\ell_{\rm e} = \frac{1}{3}m_{\rm e}c\sigma_{\rm T}R^2\int_1^\infty {\rm d}\gamma(\gamma-1)Q_{\rm e}$ (see MK95)
- the effective escape time $t_{\rm esc}$ of relativistic electrons, which can be identified as the timescale over which adiabatic expansion losses limit the accumulation of relativistic electrons within the source.

In terms of these parameters, the equation governing the evolution of the electron distribution $n_{\rm e}$ is:

$$\frac{\partial n_{\rm e}(\gamma,t)}{\partial t} + \frac{n_{\rm e}(\gamma,t)}{t_{\rm esc}} = Q_{\rm e}(n_{\rm e},n_\gamma,\gamma,t) + L_{\rm e}(n_{\rm e},n_\gamma,\gamma,t) \quad (1)$$

Here $L_{\rm e}$ denotes the electron loss terms (i.e., synchrotron losses and inverse Compton scattering), while $Q_{\rm e}$ is the injection term. In all cases discussed in this paper the contribution of photon–photon pair production to both photon absorption and electron injection is negligible, so that $Q_{\rm e}$ is essentially a function of only γ and t. The normalisation used is one in which time is measured in units of the light crossing time of the source (of size R) and the particle density refers to the number contained in a volume element of size $\sigma_{\rm T}R$. All quantities are measured in the rest frame of the blob. The corresponding equation for the photon distribution n_γ reads:

$$\frac{\partial n_\gamma(x,t)}{\partial t} + n_\gamma(x,t) = Q_\gamma(n_\gamma,n_{\rm e},x,t) + L_\gamma(n_\gamma,n_{\rm e},\gamma,t) \quad (2)$$

where here $Q_\gamma(n_\gamma,n_{\rm e},x,t)$ represents the source terms for photons of frequency $\nu = xm_{\rm e}c^2/h$ (i.e., synchrotron radiation and inverse Compton scattering) and $L_\gamma(n_\gamma,n_{\rm e},\gamma,t)$ the loss term, which arises from photon-photon pair production and is negligibly small in the current application. The source and loss terms are discussed in detail in MK95. Using the above parameters in the code it is possible to fit to the multiwavelength spectrum as reported in Macomb et al. (1995, 1996) during both the quiescent and the flaring stages.

3. Fits to the multiwavelength spectrum of Mkn 421

3.1. The quiescent state

The seven parameters $\ell_{\rm e}$, s, $\gamma_{\rm max}$, δ, R, b, and $t_{\rm esc}$ are strongly constrained by the observations. In the case of Mkn 421, both the X-ray emission and the TeV emission are rapidly variable (see Macomb et al. 1995, Takahashi et al. 1995, Schubnell et al. 1996). Radio frequency photons, however, exhibit a quiescent spectrum. Since the time required for electrons to cool by synchrotron emission to energies at which they emit substantial numbers of infra-red photons is excessively long, we assume that either adiabatic expansion of the blob or escape from the source intervenes to limit the time over which a given electron radiates in this frequency range. Then the observed infra-red

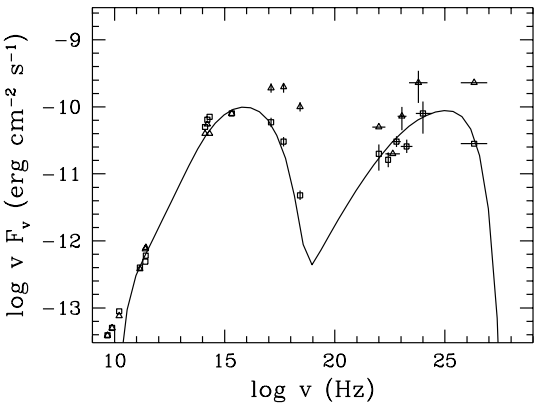

Fig. 1. The predicted and observed emission from Mkn 421 during its quiescent state. Squares indicate observations during the quiescent phase. Triangles are observations during the flaring state (Macomb et al. 1996). For the adopted parameters see text.

to radio spectral index $\alpha \approx 0.35$ is directly related to s by the well-known formula $\alpha = (s-1)/2$.

Although variable, the general form of both the X-ray and gamma-ray spectra indicates that in the SSC model synchrotron photons are emitted up to a maximum frequency of approximately 10^{18} Hz while inverse Compton photons are present up to at least 10^{27} Hz. Denoting these frequencies by $\nu_{s,18}\times 10^{18}$ Hz and $\nu_{c,27}\times 10^{27}$ Hz, respectively, we have

$$\delta b\gamma_{\rm max}^2 \approx 10^{-3}\nu_{s,18} \quad (3)$$

$$\delta\gamma_{\rm max} \approx 3\times 10^{6}\nu_{c,27} \quad (4)$$

(MK95). Eq. (4) assumes that photons of frequency $\nu_{c,27}$ are produced by inverse Compton scatterings in the Klein-Nishina regime. From these expressions we can immediately deduce $\gamma_{\rm max}$ and the magnetic field strength in terms of the (as yet undetermined) Doppler factor δ:

$$\gamma_{\rm max} = 3\times 10^{6}\nu_{c,27}\delta^{-1} \quad (5)$$

$$B = 5\times 10^{-3}\delta\nu_{s,18}\nu_{c,27}^{-2}\ \text{gauss}\ . \quad (6)$$

The next step is to relate the observed bolometric nonthermal flux F of the source to the power injected in relativistic electrons. Using the normalisation of MK95 we require the injected electron compactness ℓ_e in the rest frame of the source to be

$$\ell_e = \frac{3\sigma_T F D_L^2}{\delta^4 R m_e c^3} \quad (7)$$

where D_L is the luminosity distance to the source given by $D_L = 2c[z+1-(z+1)^{1/2}]/H_0$ for a $q_0 = 1/2, \Lambda = 0$ cosmology; for the Hubble constant we assumed $H_0 = 75\ h$ km s^{-1} Mpc^{-1} and the redshift of Mkn 421 is $z = 0.0308$. Observations of Mkn 421 indicate that in the SSC model, the flux of synchrotron photons (i.e., those of frequency $< \nu_{s,18}$) is comparable to the flux of inverse Compton photons (those with frequency $> \nu_{s,18}$). In the rest frame of the blob, this implies approximate equality of the two compactnesses ℓ_e and ℓ_B since these quantities are proportional to the internal photon and magnetic energy density respectively. Writing $\eta = \ell_e/\ell_B$ we have

$$R = 3\times 10^{19}\ell_e\eta^{-1}B^{-2}\ \text{cm} \quad (8)$$

with B in gauss. Using Eq. (7) and the observationally derived relation $FD_L^2 \approx 6\times 10^{44}$ erg/sec, we obtain from Eq. (8)

$$R \simeq 1.2\times 10^{18}\left(\frac{FD_L^2}{6\times 10^{44}\ \text{erg/sec}}\right)^{1/2}\eta^{-1/2}B^{-1}\delta^{-2}\ \text{cm}. \quad (9)$$

The observation that the synchrotron spectrum steepens at a frequency somewhere between millimeter and optical wavelengths (Brodie, Bowyer & Tennant 1987) enables one to estimate the escape time first by calculating an effective Lorentz factor $\gamma_{\rm br}$ below which escape is faster than cooling

$$\gamma_{\rm br} \simeq \frac{3}{4\ell_B t_{\rm esc}} \quad (10)$$

and then relating this to the turnover frequency by

$$\nu_b \simeq 1.3\times 10^{20}\delta b\gamma_{\rm br}^2. \quad (11)$$

This approach gives an escape time

$$t_{\rm esc} = 8.9\times 10^{14}\delta^{1/2}B^{-3/2}R^{-1}\nu_{b,15.3}^{-1/2} \quad (12)$$

expressed in units of t_{cr}. Here $\nu_{b,15.3} = \nu_b/10^{15.3}$ Hz is the frequency of the spectral break.

Finally, the rapid variability of the X-ray and TeV emission on timescales $t_{\rm var}$ of 10^5 secs constrains the overall size of the source and the Doppler boosting factor. Thus using $t_{\rm var} = R/(c\delta)$ and eliminating B between Eqs. (6) and (9) to find the value of R, we deduce

$$\delta = 15 t_5^{-1/4} \quad (13)$$

where $t_5 = t_{\rm var}/(10^5\ \text{s})$ and we have inserted canonical values for the observed quantities.

Following the above guidelines one can allow the code to reach a stationary state and find detailed fits to the 'quiescent' multiwavelength spectrum of Mkn 421 (Macomb et al. 1995, 1996). With the exception of the slope of injected electrons s, all other parameters can be expressed in terms of the Doppler factor δ. Thus, we first use the approximate observed quantities $\nu_{s,18}$, $\nu_{c,27}$, FD_L^2, α, $\nu_{b,15.3}$, and the observed approximate equality of ℓ_e and ℓ_B, to fit the observed quiescent spectrum and subsequently adjust δ to fit the observed variation time t_5. We find a satisfactory fit using the parameters $R = 4.7\ 10^{16}\delta_{15}^{-3}$ cm, $B = .07\delta_{15}$ gauss, $\gamma_{\rm max} = 2\ 10^5\delta_{15}^{-1}$, $s = 1.7$, $\ell_e = 1.93\ 10^{-5}\delta_{15}^{-1}$ and $t_{\rm esc} = 3.3 t_{\rm cr}\delta_{15}^2$. Here $\delta_{15} = \delta/15$. Fig. 1 shows the calculated quiescent spectrum for $\delta_{15} = 1$.

3.2. The flaring state

In the present model, the simplest way to explain the flaring activity of Mkn 421 reported by Macomb et al. (1995) is to change the electron parameters q_e and/or $\gamma_{\rm max}$ or to change the magnetic field. The first two can be understood as sudden variations in the acceleration mechanism while the third corresponds to the blob entering a region of higher field strength.

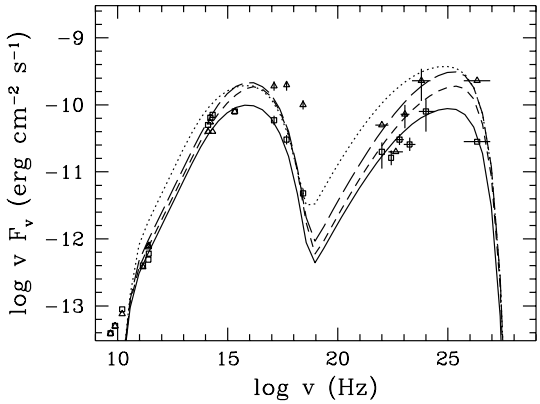

Fig. 2. Evolution of the multiwavelength spectrum of Mkn 421 in the case where the amplitude of the electron injection changes impulsively by a factor of 3. The solid line corresponds to the quiescent spectrum of Fig. 1. The short and long dashed lines show the spectrum at 1 and $2t_{\rm var}$ after the change in the electron injection (corresponding to 1.2 and 2.4 days respectively). The dotted line shows the new steady state which, however, is achieved many $t_{\rm var}$ later.

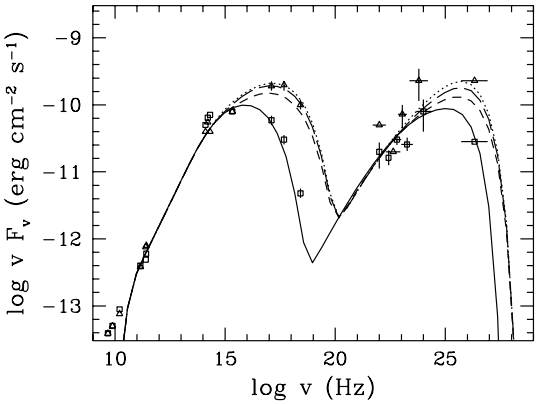

Fig. 4. Evolution of the multiwavelength spectrum of Mkn 421 in the case where the maximum energy of the electrons $\gamma_{\rm max}$ changes impulsively by a factor of 5. The solid line corresponds to the quiescent spectrum of Fig. 1. The short and long dashed lines show the spectrum at 1 and 2 $t_{\rm var}$ after the change in the electron injection (corresponding to 1.2 and 2.4 days respectively). The dotted line shows the new steady state.

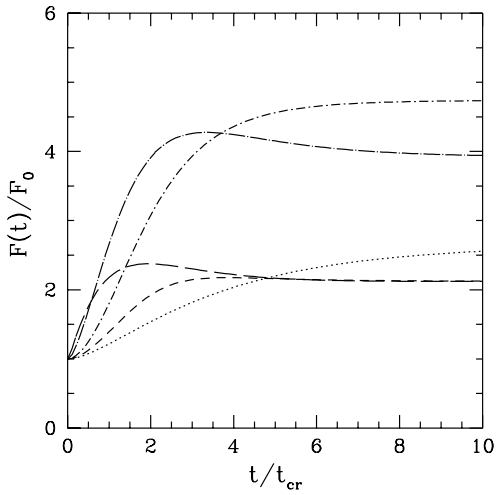

Fig. 3. Plot of the flux at various frequencies (normalised to its quiescent value) for the flare that corresponds to a change in $q_{\rm e}$ by a factor of 3 over the quiescent state. The dotted line corresponds to a wavelength of 0.4 cm, the small dash line to optical wavelengths, the large dash line to 2-10 keV X-rays, the small dot-dash line to .1-30 GeV γ-rays while the large dot-dash line to $\geq$ 500 GeV γ-rays.

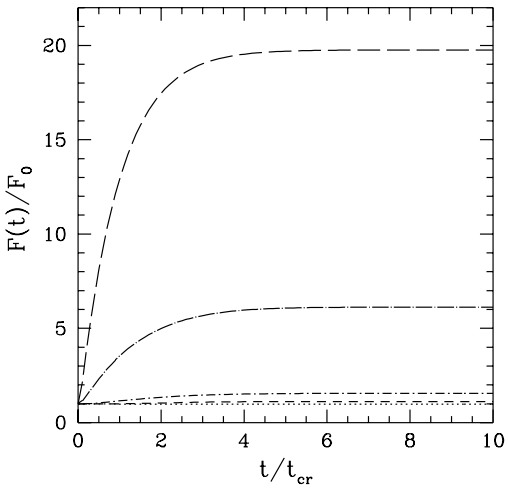

Fig. 5. Plot of the flux at various frequencies (normalised to its quiescent value) for the flare that corresponds to a change in $\gamma_{\rm max}$ by a factor of 5. The dotted line corresponds to a wavelength of 0.4 cm, the small dash line to optical wavelengths, the large dash line to 2-10 keV X-rays, the small dot-dash line to .1-30 GeV γ-rays while the large dot-dash line to $\geq$ 500 GeV γ-rays.

3.2.1. Flares due to changes in $q_{\rm e}$

Fig. 2 shows how a flare evolves in the case in which the amplitude of the electron injection spectrum $q_{\rm e}$ is suddenly increased by a factor of 3 above the quiescent value found in the previous section and then left constant. The short and long dashed lines correspond to snapshots of the spectrum after 1 and $2t_{\rm var}$, respectively, measured from the time at which $q_{\rm e}$ changed ($t_{\rm var} \simeq 1.2$ days). The dotted line corresponds to the new steady state, which is achieved many days later. It is evident that a change in $q_{\rm e}$ produces prompt flaring activity in the UV/X-ray and TeV $\gamma-$ray bands. This can be attributed to the fact that high energy electrons have shorter cooling times than low energy ones. Therefore the newly injected high amplitude electron distribution cools first at the high frequency end, producing synchrotron X-rays and inverse Compton TeV gamma-rays. The lower frequency photons (optical synchrotron and GeV gamma-rays) lag behind somewhat. This can be better seen in Fig. 3, which shows the lightcurves of various frequency bands as a function of time (the travel crossing time across the emitting region has not been

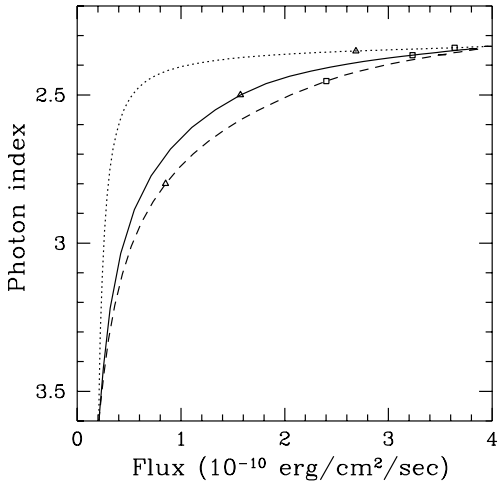

Fig. 6. Plot of the 2-10 keV photon index as a function of the flux at the same energy band that corresponds to a change in $\gamma_{\rm max}$ by a factor of 5. The dotted line corresponds to an impulsive change in $\gamma_{\rm max}$, while the full and dashed lines correspond to a more gradual change with the change completed in the first case in one $t_{\rm var}$ and in $2t_{\rm var}$ in the second. The triangles and squares indicate the values at 1 and $2t_{\rm var}$ respectively.

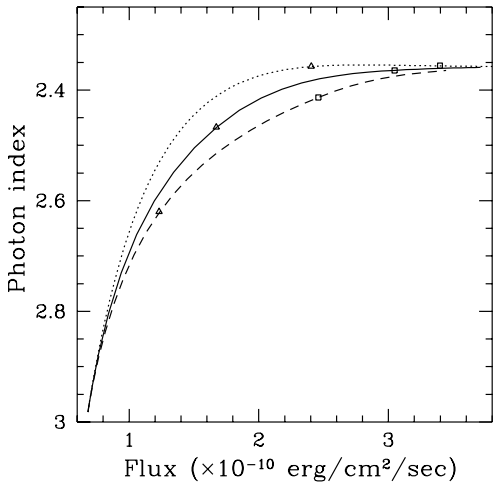

Fig. 7. Plot of the $\geq$ 500 GeV photon index as a function of the flux at the same energy band that corresponds to a change in $\gamma_{\rm max}$ by a factor of 5. The dotted line corresponds to an impulsive change in $\gamma_{\rm max}$, while the full and dashed lines correspond to a more gradual change with the change completed in the first case in one $t_{\rm var}$ and in $2t_{\rm var}$ in the second. The triangles and squares indicate the values at 1 and $2t_{\rm var}$ respectively.

taken into account). The X-rays have the fastest response while the optical shows a slower response. Similarly TeV radiation has a faster response than GeV radiation. Note also that the amount by which the synchro-Compton component increases is larger than that by which the synchrotron component rises, since the latter varies approximately as proportional to $q_{\rm e}^2$ whereas the former is roughly proportional to $q_{\rm e}$. [1] However, this holds only if the change in $q_{\rm e}$ lasts long enough for a new quasi steady state to be established. If, for example, the electron injection is turned off after one crossing time, this effect will not be observed. Finally, it can be seen from Fig. 2, that although the predicted flare matches the observed increase in amplitude as observed by Whipple, it does not reproduce the hard X-ray spectral shape. In addition, the model underestimates the high X-ray flux by at least one order of magnitude.

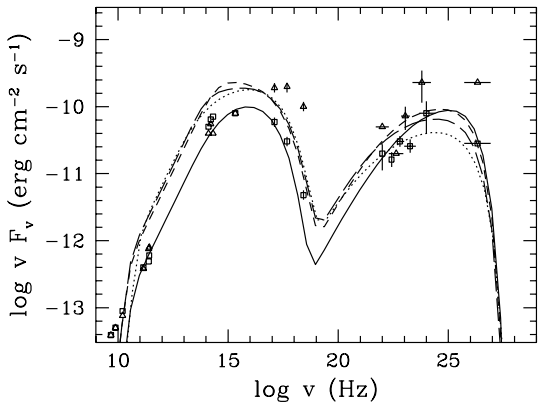

Fig. 8. Evolution of the multiwavelength spectrum of Mkn 421 in the case where the magnetic field strength changes impulsively by a factor of 3 and then left constant. The solid line corresponds to the quiescent spectrum of Fig. 1. The short and long dashed lines show the spectrum at 1 and 2 $t_{\rm var}$ after the change in the electron injection (corresponding to 1.2 and 2.4 days respectively). The dotted line shows the new steady state.

3.2.2. Flares due to changes in $\gamma_{\rm max}$

The evolution of a flare which corresponds to an impulsive increase of $\gamma_{\rm max}$ by a factor of 5 is shown in Fig. 4. Once again the short and long dashed lines correspond to snapshots of the spectrum after 1 and 2 $t_{\rm cr}$ respectively as measured from the time of the sudden change in $\gamma_{\rm max}$. The final steady state is shown as a dotted line and it is reached after roughly $3t_{\rm cr}$. In contrast to the previous case, the predicted flaring activity due to an increase in $\gamma_{\rm max}$ gives a good fit both in X-rays and TeV $\gamma-$rays. Fig. 5 displays the light curves predicted in frequencies from infra-red to hard gamma-rays. The evolution of the flare is very different from the previous case as here the source exhibits an outburst only in X-rays and TeV $\gamma-$rays while the other frequencies remain practically unaffected. This behaviour was also found by Marscher & Travis (1996) and it was suggested by Macomb et al. (1995) as a possible interpretation of their data. Note that the variability in the GeV range is of the same order as the size of the error bars. Furthermore we find that, contrary to the previous case, the X-ray flare is of higher amplitude than the TeV one.

[1] In the present model self-consistent electron cooling is included by both synchrotron and inverse Compton losses. This breaks the simple linear dependence of synchrotron flux on $q_{\rm e}$.

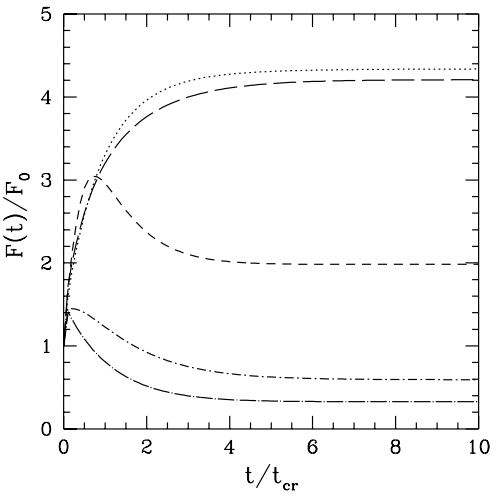

Fig. 9. Plot of the flux at various frequencies (normalised to its quiescent value) for the flare that corresponds to a change in magnetic field strength by a factor of 3. The dotted line corresponds to a wavelength of 0.4 cm, the small dash line to optical wavelengths, the large dash line to 2-10 keV X-rays, the small dot-dash line to .1-30 GeV γ-rays while the large dot-dash line to $\geq$ 500 GeV γ-rays.

From Fig. 5 it is also evident that in this case the outburst is strongest in the X-ray regime. In fact, there are marked changes in the spectral index of the X-rays during a flare. This is displayed in Fig. 6, which plots the 2–10 keV spectral index as a function of flux in this energy range. Three different flares are plotted, which differ in the time scale over which $\gamma_{\rm max}$ is increased: first of all impulsively (dotted line), then on a time scale of $t_{\rm var}$ (solid line) and then $2t_{\rm var}$ (dashed line). In each case a spectral hardening in X-rays with increasing flux is predicted, in qualitative agreement with recent ASCA observations (Takahashi et al. 1995). A similar effect can be observed in the hard gamma-ray (> 500 GeV) range. This is shown in Fig. 7.

3.2.3. Flares due to changes in B

As a final example, we present a flare caused by a sudden increase in the strength of the magnetic field. Fig. 8 depicts the spectral evolution that corresponds to an impulsive increase of the magnetic field strength by a factor of 3 and then left there. In this case, the whole synchrotron spectrum is shifted to the right by the same factor and is also boosted in intensity, as might be expected. The synchro-Compton component, on the other hand, is reduced compared to its original steady state value. The reason is that the ratio $\ell_{\rm e}/\ell_{\rm B}$ is reduced when the field increases, so that the total luminosity (which is held constant) is redistributed towards the synchrotron component. This behaviour can also be seen in Fig. 9 where one can observe a fast increase in the flux of low frequency bands along with a decrease of the flux in the γ-ray bands. This result contrasts strongly with similar investigations by Bloom & Marscher (1996). There is, however, no discrepancy, since these authors consider a change in the magnetic field whilst holding the electron *distribution* constant. In our case, we keep the electron injection (and hence the total luminosity) constant.

4. Discussion

In the present paper we obtained fits to the X-ray/TeV flares observed during the 1994 multiwavelength campaign of Mkn 421 in the context of the homogeneous synchro-Compton model. This model assumes that the most important photon targets for inverse Compton scattering by relativistic electrons are the synchrotron photons they themselves produce. In the case of BL Lac objects such as Mkn 421, this assumption may be justified, since there is no evidence of a more important photon component. However, this may not be the case in other sources, where photons from an accretion disk (Dermer, Schlickeiser & Mastichiadis 1992) or photons scattered from broad line clouds (Sikora, Begelman & Rees 1994) may dominate. Nevertheless, a combination of synchrotron radiation and inverse Compton scattering on external photons (Dermer, Sturner & Schlickeiser 1996) may be useful in modelling results such as those of the multi-wavelength campaign on 3C273 (Lichti et al. 1995). Whether a homogeneous synchro-Compton model such as presented here can explain these or similar observations (e.g., those of 3C279: Maraschi et al. 1994, Hartman et al. 1996) is currently under investigation.

We obtain the full time dependent behaviour of flares by fitting the 'quiescent' spectrum of the source and then varying one of the free parameters. Three simple ways of producing flares were investigated: (i) by changing the amplitude of the electron injection spectrum, (ii) by changing the maximum energy of the electron injection spectrum and (iii) by changing the magnetic field strength. We found a good fit to the observations using a flare of type (ii). This produces changes only in the X-ray and TeV bands, leaving all the other bands essentially unaffected. It also reproduces qualitatively the observed hardening of the X-rays with increasing intensity (Takahashi et al. 1995). We also found that X-rays are first to react to any change in the electron injection. This is particularly pronounced for flares of type (i) and (ii) (see Figs. 3 and 5). A change in the acceleration parameters is tracked more closely by X-ray photons than by photons in other wave-bands, since the X-ray producing electrons have the highest energy and, therefore, the the fastest cooling timescale.

The parameters we find for the fits are similar to those found by other authors (see, for example, Marscher & Travis (1996), Sambruna, Maraschi & Urry (1996)). The fast time variability of Mkn 421 ($\simeq$1 day) implies a Doppler factor of $\simeq$15. However, a faster variation can easily be accommodated in our model, since new fits with a larger Doppler factor can be obtained simply scaling the parameters as indicated in Sect. 3. One potentially independent constraint on the model is provided by the effects of synchrotron self-absorption. At the lower radio frequencies, the absorption turnover can be seen in Figs. 1, 2, 4 and 8. For higher Doppler factors, this effect should disappear, since the required luminosity is then provided by a lower value of $\ell_{\rm e}$. As a result, the electron column density of the source is reduced. However, the homogeneous SSC model presented here is so compact that

the effects of induced Compton scattering can also be expected to manifest themselves in the radio range (Coppi, Blandford & Rees 1993, Sincell & Krolik 1994). A simple estimate of the importance of this effect can be obtained by evaluating the parameter $\tau_{\rm ind} = N_{\rm e}\sigma_{\rm T}RT_{\rm br}/(m_{\rm e}c^2)$, where $T_{\rm br}$ is the brightness temperature of the radiation in energy units and $N_{\rm e}$ is the total electron density in the source. Even if we assume that no thermal electrons are present, this parameter exceeds unity for frequencies less than roughly 700 MHz, given the parameters of our quiescent model. Thermal electrons, however, accumulate within the source, although we have not calculated their density explicitly. consequently, a modification of the simple synchrotron spectrum at gigaherz frequencies may be possible.

Our calculations predict the time-dependent flaring activity to be expected given certain idealised fluctuations in the injection spectrum of high energy electrons into a relativistically moving blob. Although we do not address a specific acceleration mechanism, it is possible to interpret the overall picture as one in which a shock front rapidly accelerates electrons and leaves a trail of them (i.e., injects them) in the plasma streaming away from the shock on its downstream side. In our model, we assume the typical dimension of the radiating part of the downstream plasma in its rest frame is R. The photon escape time is $t_{\rm cr}$, which we find to be roughly one third of the time taken for electrons to cross the emitting region. Thus, assuming electrons are carried along by the plasma, our picture would indicate rapid ($\sim c/3$) movement of the downstream plasma away from the shock front. In a more realistic model, the spectrum of injected electrons should also be calculated in a time-dependent manner. In fact, the value of $\gamma_{\rm max}$ itself should probably be determined by a balance between acceleration and losses in a self-consistent model. This is possible in a hadronic model (e.g., MK95), however, self-saturation of accelerated protons requires a very high photon density, which would render the source opaque to TeV gamma-rays. On the other hand, it is possible to imagine a model in which protons saturate at extremely high energy (e.g., Mannheim 1993), and inject electrons which produce the entire emitted spectrum by the synchrotron mechanism. The time-dependent properties of flares from such a model would, however, differ strongly from those found above. A detailed investigation of electron acceleration in the presence of losses (Heavens & Meisenheimer 1987) has so far been performed only in the steady state, and without considering either bulk relativistic motion or inverse Compton scattering.

Another simplification we have introduced comes from the fact that we have used a spherical homogeneous model (for a discussion of the problems inherent with this model see, for example, Bloom & Marscher 1996). However this allows us to understand better the significance of the various physical quantities we are using and, at least for the case of Mkn 421, it proved adequate to fit the multiwavelength spectrum. On the other hand, the inhomogeneous models might be superior to the homogeneous ones in the sense that they give better overall fits to the AGN spectra, however they introduce a number of extra parameters making a simple understanding of the results difficult.

Acknowledgements. We would like to thank an anonymous referee who helped us clarify many of the issues presented here. AM thanks the Deutsche Forschungsgemeinschaft for support under Sonderforschungsbereich 328.

References

Blandford, R.D., Levinson, A. 1995, ApJ 441, 79
Bloom S.D., Marscher A. 1996 ApJ 461, 657
Brodie J., Bowyer S., Tennant A. 1987, ApJ 318, 175
Celotti, A., Maraschi, L., Treves, A. 1991, ApJ 377, 403
Coppi, P., Blandford, R.D., Rees, M.D. 1993, MNRAS 262, 630
Dermer, C.D., Schlickeiser, R., Mastichiadis, A. 1992, A&A 256, L27
Dermer, C.D., Schlickeiser, R. 1993, ApJ 416, 458
Dermer, C.D., Sturner,S., Schlickeiser, R. 1996, preprint
Ghisellini, G., Maraschi, L., Treves, A. 1985, A&A 146, 204
Hartman, R.C., ApJ, in press.
Heavens, A.F., Meisenheimer, K. 1987, MNRAS 225, 335
Jones, T.W., O'Dell, S.F., Stein, W.A. 1974, ApJ 188, 353
Lichti, G.G., et al. 1995, A&A 298, 711
Macomb, D.J. et al. 1995 ApJ 449, L99
Macomb, D.J. et al. 1996 ApJ 459, L111 (Erratum)
Makino, F. et al. 1987, ApJ 313, 662
Mannheim, K. 1993, A&A 269, 67
Maraschi L., Ghisellini G., Celotti A. 1992, ApJ 397, L5
Maraschi, L. et al. 1994, ApJ 435, L91
Marcowith, A., Henri, G., Pelletier, G. 1995, MNRAS 277, 681
Marscher, A.P., Travis, J.P., 1996 A&A Suppl, in press
Mastichiadis A., Kirk, J.G., 1995 A&A 295, 613 (MK95)
Punch, M. et al. 1992, Nature 358, 477
Sambruna, R.M., Maraschi, L., Urry, C.M. 1996, ApJ 463, 444
Schubnell, M. et al. 1996, ApJ 460, 644
Sikora, M., Begelman, M.C., Rees, M.J. 1994, ApJ 421, 153
Sincell, M.W., Krolik, J.H. 1994, ApJ 430, 550
Takahashi, T. et al. 1995, ApJ Letters, in press
von Montigny, C., et al. 1995, ApJ 440, 525

This article was processed by the author using Springer-Verlag LaTeX A&A style file *L-AA* version 3.